PERGAMON

International Journal of Solids and Structures 37 (2000) 1931–1949

INTERNATIONAL JOURNAL OF SOLIDS and STRUCTURES

www.elsevier.com/locate/ijsolstr

The in-plane non-linear compression of regular honeycombs

H.X. Zhu, N.J. Mills*

School of Metallurgy and Materials, University of Birmingham, Birmingham B15 2TT, UK

Received 17 July 1998; in revised form 6 November 1998

Abstract

A theoretical analysis is made of the in-plane uniaxial compression of regular honeycombs made from a range of materials. Both the elastic and elastic-plastic responses are considered, as a function of the honeycomb density, for strains until the faces touch. The stress–strain relationship and lateral expansion are predicted for loading in the symmetry axis directions, for deformation modes with and without vertex rotation. For an elastic honeycomb, compressed parallel to one set of faces, a buckling mode with vertex rotation gives the lower stress, for strains exceeding 10% in honeycombs with single thickness vertical faces, and 15% strain for double-thickness faces. If the material yields, or other forms of non-linearity occur, there can be strain softening, which leads to strain localisation. Deformation mechanisms are linked to the material response and the honeycomb density, and are compared with experiments on polymeric honeycombs.

Keywords: Honeycomb; Non-linear deformation; Polymers; Buckling

1. Introduction

A variety of materials are now available as honeycomb structures. Aluminium, paper and 'Nomex' honeycombs are made by expanding bonded sheet material (Bitzer, 1997). More recently polypropylene has been extruded with a honeycomb section, and rubbery thermoplastics have been injection moulded. These materials have quite different stress strain responses from aluminium alloys, and have higher elastic strains. The in-plane compression of regular honeycomb structures has been analysed by El-Sayed et al. (1979), Gibson et al. (1982), Papka and Kyriakides (1994), and Masters and Evans (1996), but the approaches either involve restrictions to the linear range of behaviour, or Finite Element Analysis (FEA) has been used for a specific material and honeycomb density. Honeycomb analysis has been

* Corresponding author. Tel.: 0121-414-5185; fax: 0121-414-5232.
E-mail address: n.j.mills@bham.ac.uk (N.J. Mills)

0020-7683/00/$ - see front matter
PII: S0020-7683(98)00324-2

justified as a proving ground for the development of the micromechanics of foams (Warren and Kraynik, 1987). However the deformation mechanisms for the high-strain compression polystyrene foams (biaxial face loading with tensile yield in one direction, and elastic-plastic buckling in the other) observed by Mills and Zhu (1999) are significantly different from those in aluminium honeycomb (elastic bending of faces followed by localised plastic bending).

The geometrically non-linear deformation of units, consisting of three honeycomb half-faces joined at 120° at a vertex, was considered by Warren et al. (1989). These units are pin connected, so the face loading conditions can differ from those in a regular honeycomb once buckling occurs. Zhu et al. (1997) used the Elastica approach to analyse the high-strain elastic compression of an open-cell Kelvin foam. It will be used here for some modes of elastic deformation of 'regular' honeycombs (the cells are regular hexagons with 120° angles). For a long, thin strut the deflections due to shear or axial compression can be neglected compared with those due to bending (Timoshenko and Gere, 1961). Therefore, for low-

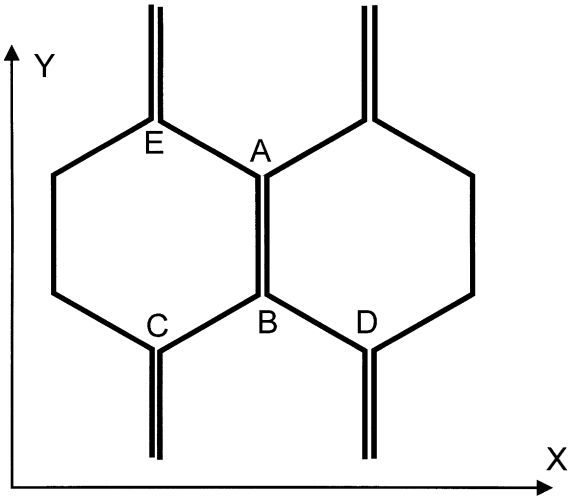

Fig. 1. Schematic of expanded honeycomb, with the double thickness faces aligned with the y-direction.

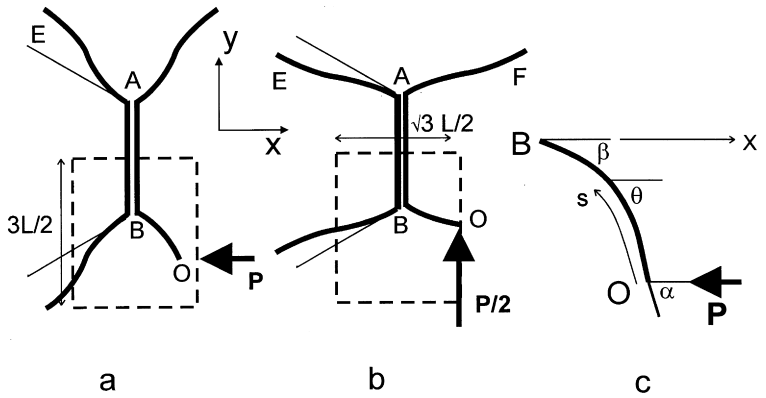

Fig. 2. Compression of honeycombs (a) in the x-direction, (b) in the y-direction without vertex rotation (mode 1), (c) a cantilever half face bending under the force P. After Gibson and Ashby (1988) but redrawn.

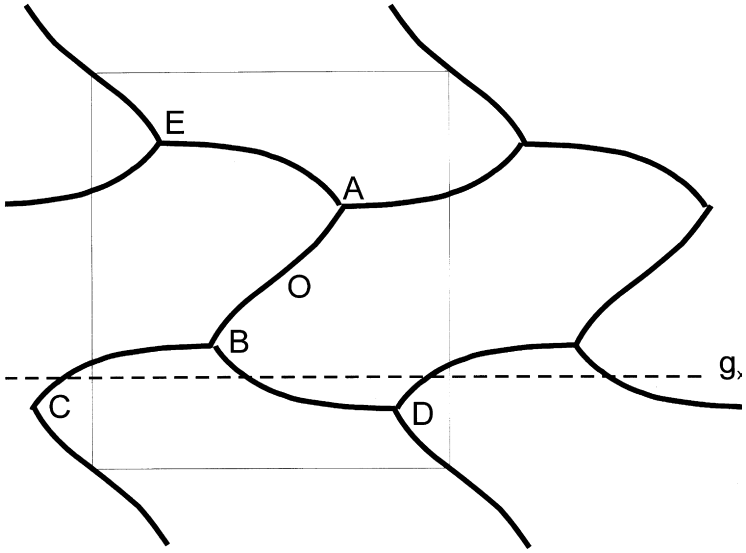

Fig. 3. Compression of a honeycomb in the y-direction, with neighbouring vertices rotating in opposite directions (mode 2). The rectangular unit cell is outlined, and the glide plane in the x-direction shown as a dashed line. The shape is a prediction for 30% strain. After Gibson and Ashby (1988) but recalculated.

density honeycombs, face bending is the dominating deformation mechanism for in-plane compression, unless there is equal biaxial compression.

For expanded honeycombs, where faces of double thickness are parallel, the y-axis is chosen to lie in this plane (Fig. 1). For compression in the x-direction (Gibson and Ashby, 1988), the faces containing the y-axis are stress free, so the deformation is limited to the slanting faces (Fig. 2a). For compression in the y-direction, the vertical faces are under compression, but in the mode 1 deformation pattern they do not bend (Fig. 2b). At higher strains, and mode 2 deformation pattern develops (Gibson and Ashby, 1988) in which all the faces deform by bending, and neighbouring vertices rotate in opposite directions (Fig. 3).

El-Sayed et al. (1979) analysed the in-plane Young's modulus of honeycombs, and the collapse stress when plastic hinges form at the ends of the single-thickness faces. Gibson et al. (1982) extended this analysis, and established clearly the moduli and collapse stresses of honeycombs. They confirmed El-Sayed et al.'s result that the initial Young's modulus of a regular honeycomb E_{HC} (with equal thickness faces) is isotropic in the plane, related to the face thickness t to length L ratio by

$$E_{HC} = \frac{4}{\sqrt{3}} E \left(\frac{t}{L} \right)^3 \tag{1}$$

For low-density honeycombs of uniform wall thickness, where the volume of the vertices can be ignored, the relative density R is given by

$$R = \frac{2}{\sqrt{3}} \frac{t}{L} \tag{2}$$

so the Young's modulus of a regular honeycomb is related to its relative density by

$$E_{HC} = 1.5 E R^3 \tag{3}$$

This result can be used as a check on the validity of low-strain computations. They experimented with silicone rubber honeycombs, loaded uniaxially in the y-direction, and observed that, when elastic collapse occurred, neighbouring vertices rotated by angles of $\pm\phi$. This deformation mode was the basis of their elastic buckling analysis, which considered the initially vertical faces AB (Fig. 1), restrained at the ends by rotational springs of a constant stiffness. They calculated an Euler buckling load for the onset of buckling; no attempt was made to calculate the compressive stress at higher strains, when the cell face shape has changed. Therefore the effects of geometric non-linearity were not considered. The predicted elastic collapse stress σ_{CE} of a regular honeycomb, with uniform thickness faces, is

$$\sigma_{CE} = \frac{0.343^2\pi^2}{3\sqrt{3}} E\left(\frac{t}{L}\right)^3 = 0.223E\left(\frac{t}{L}\right)^3 \tag{4}$$

They commented that the small change in cell wall angle prior to buckling changes the result by less than 10%, less than the variation in experimental data. Gibson and Ashby (1988) divided the elastic buckling stress of eqn (4) by the Young's modulus of eqn (1) to estimate that buckling initiated at a strain of 10%. This assumes that the stress–strain curve remains linear to the point of buckling. In their analysis of plastic collapse for stresses in the x- or y-directions, it is assumed that the vertices do not rotate, and that the faces only bend at the plastic hinges. The predicted stress for collapse by yielding is, for both stress directions

$$\sigma_{CY} = \frac{2}{3}\sigma_0\left(\frac{t}{L}\right)^2 \tag{5}$$

Their analysis does not give the yield strain, or details of the stress–strain curve.

Klintwood and Stronge (1988) assumed that the double-thickness cell faces (plus a layer of adhesive) of expanded honeycombs were rigid, and considered both elastic buckling and plastic collapse under plane stress loading. This paper will consider the error introduced by their approximation. For uniaxial compression their equation, for the y-direction stress to initiate mode 2 buckling, reduces to

$$\sigma_{CE} = 0.346\frac{\pi^2}{6\sqrt{3}} E\left(\frac{t}{L}\right)^3 = 0.328E\left(\frac{t}{L}\right)^3 \tag{6}$$

Using eqn (1) for the honeycomb Young's modulus, the strain at buckling can be estimated as 0.142.

Papka and Kryriades (1994) presented FEA results for the compression of an aluminium honeycomb with double-thickness vertical faces. When they assumed an elastic material for uniaxial compression, the elastic buckling strain was just over 15%, although they did not comment on the value. The boundary conditions (not specified) were presumably periodic in both the x- and y-directions, to allow the alternating vertex rotation. They also made an elastic-plastic FEA analysis, in which the slope of the aluminium stress–strain curve fell by a factor of 100 once the yield strain of 0.423% was exceeded. Collapse was by plastic hinge formation in the slanting faces close to the vertices, at a compressive strain of 5% (for a honeycomb with a t/L ratio of 0.0264). When they varied the aluminium yield strain from 0.3 to 1%, the 'limit stress' for the onset of plastic collapse increased almost linearly. For the 0.3% yield strain, the predicted yield stress was given by eqn (5) but, for the 1% yield strain, the predicted stress was 90% of the value from eqn (5), probably due to their consideration of the elastic face deformation. Their results, for a specific material and for a honeycomb of a specific density, cannot be generalised for other materials and densities. In their experiments on aluminium honeycombs, neighbouring vertices were observed rotate in opposite directions. It is of interest to see if this rotation affects the predicted plastic collapse stress. A high-strain deformation band developed, perpendicular to the stress axis. This band then propagated into the neighbouring layers of cells.

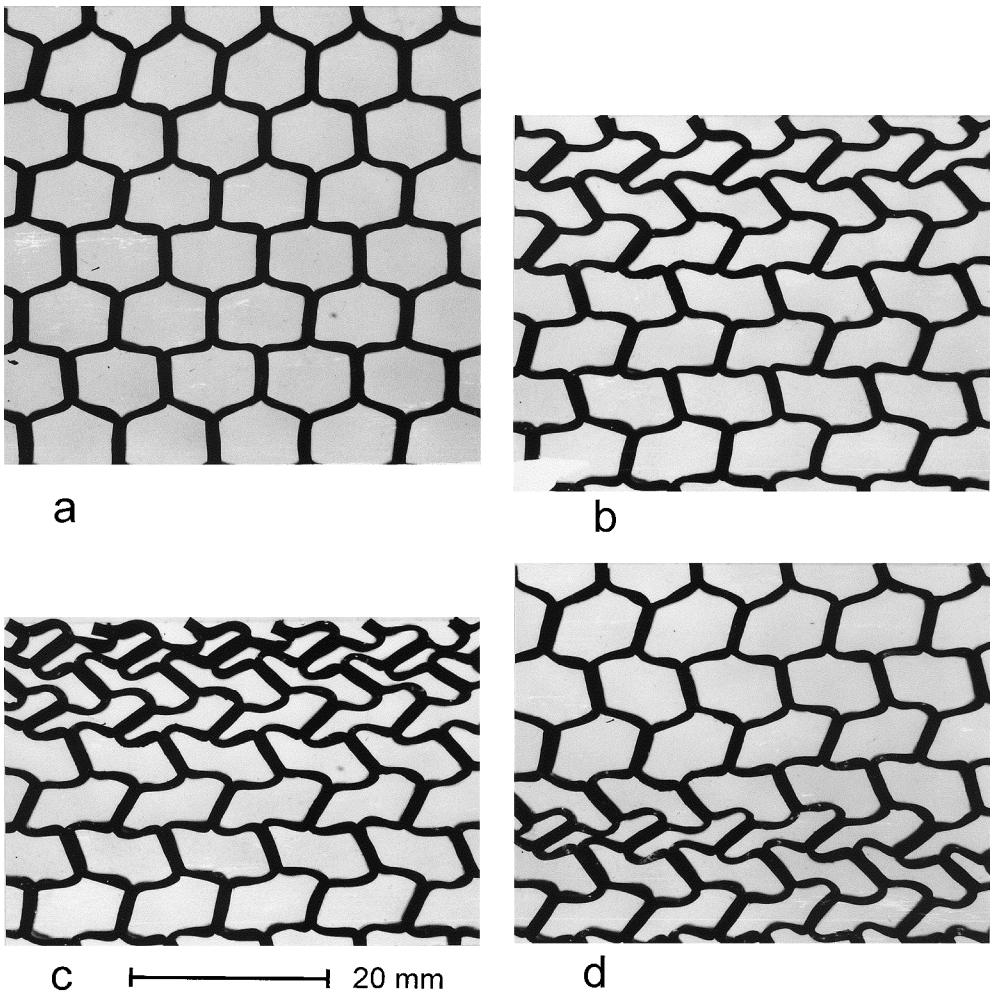

Fig. 4. Thermoplastic elastomer polymer honeycomb under uniaxial compression to strains of (a) 10%, (b) 30%, (c) 40%, (d) unloaded to 30% strain.

Hutzler and Weaire (1997) analysed the biaxial in-plane compression of honeycombs with uniform thickness faces. They imposed a strain in the y-direction, then adjusted the x-axis strain to minimise the elastic energy of the honeycomb. They calculated that a compressive strain of 8% would initiate the mode 2 elastic buckling pattern similar to that in Fig. 3. However, they could not use this energy approach to model uniaxial compression.

The goals of this paper are to find the effects of varying material parameters on the elastic and plastic collapse of honeycombs of a range of densities, and to classify the preferred deformation modes. By considering both material and geometric non-linearity, the effects of each on the shape of the stress–strain curve can be separated.

2. Experimental compression of polymer honeycombs

Two commercially available honeycombs were tested. The first is a thermoplastic-elastomer (TPE) honeycomb, used as part of a cycle helmet, and the second is a polypropylene honeycomb, tradename Nida-Core, which is used as the core of fibreglass or wood veneer sandwich structures. The dimensions of the honeycombs are given in Table 1. Fig. 4 shows the deformation of the TPE honeycomb under uniaxial compression in the y-direction. It is 3.1 mm thick and 46 mm high, so is constrained between glass faces to prevent it from buckling out of the plane. The sample is cut so that the compressive force is applied to the midpoints of vertical faces, so the end constraints are as near as possible those of an infinite honeycomb. However, the cells at the corners of the honeycomb have slightly different constraints, and friction increases at the honeycomb/glass interface when high strains occur in the honeycomb. The load was applied through 3 mm thick rectangular blocks of polycarbonate that could slide between the restraining glass plates. The strain was determined from the directly measured crosshead motion of the Instron testing machine. The shape of the deformed honeycombs was photographed using a 90 mm focal length Nikon macro lens.

At a compressive strain of 10% the mode 1 deformation pattern occurs in cells near the centre of the honeycomb (Fig. 4a). Mode 2 deformation is visible in these cells when the strain is 15 or 20%. At a 30% average strain (Fig. 4b) layers of cells near the top of the sample become more highly deformed, so strain is inhomogeneous. By 40% strain (Fig. 4c) the opposite sides of these cells touch, limiting the local strain to about 70%, and effectively hardening the layer of cells. At higher average strains this highly-deformed region propagates through the honeycomb, in the same way that a neck propagates in a tensile test in a polymer specimen. On unloading from a maximum of 55% strain, there is strain inhomogeneity in the recovery process (Fig. 4d), possibly as a result of interface friction. The polypropylene honeycomb of limited size (18 mm thick and 40 mm high) did not have to be constrained. A total of 6 faces in the 26 complete cells were buckled before testing, causing cells to collapse at random positions when the honeycomb was compressed. There was no regularity in cell shapes at 50% strain. The honeycomb recovered its overall shape with three more buckled faces, which recovered in a period of hours.

Table 1
Thermoplastic honeycombs tested

Material	Cell face length mm	Cell face thickness mm	Vertical faces	Compressive collapse stress kPa
TPE	4.3	0.4 ± 0.1	Double	2.5
Polypropylene	5.1	0.3 ± 0.05	Single	15

Fig. 5a shows the compressive stress–strain curve for the TPE honeycomb and Fig. 5b the tensile stress–strain curve for the elastomer. The shape of the loading and unloading curves were similar to those of a polyurethane which was found to be non-linearly viscoelastic (by carrying out stress relaxation experiments from a range of initial strains). The apparent Young's modulus is 40 MPa at the start of the loading curve, which was at a nominal strain rate of 3.7×10^{-3} s^{-1}. Hysteresis occurs when high-strain deformation bands are propagating or unfolding in the honeycomb at average strains in excess of 30%, possibly due to interface friction. The initial collapse stresses of the polypropylene

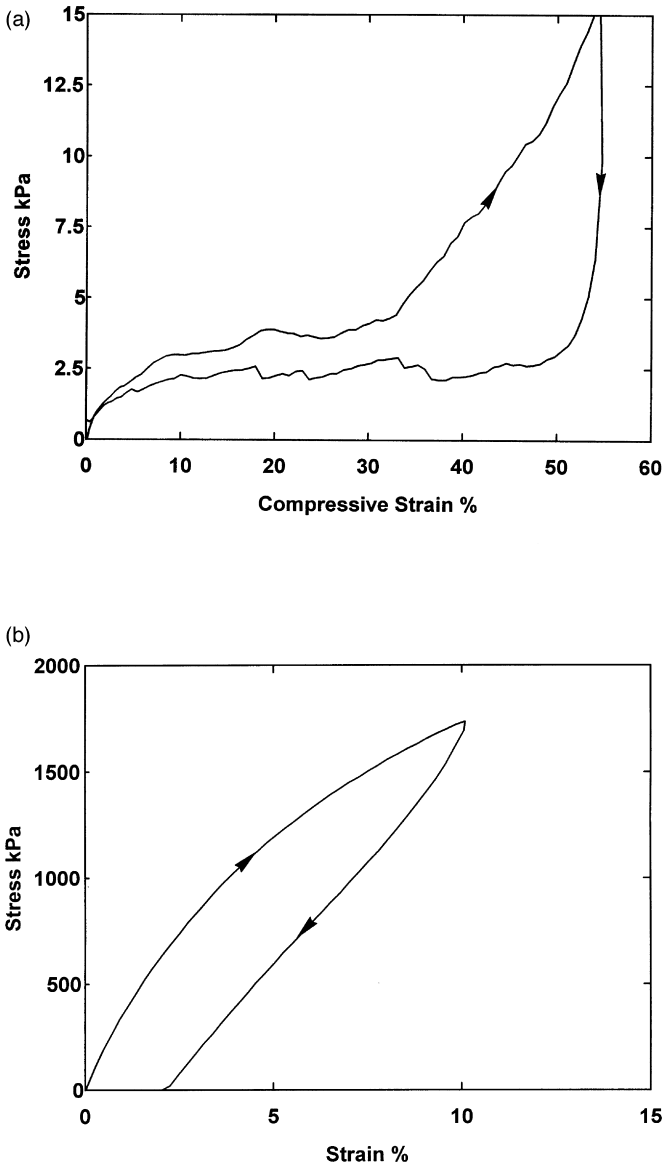

Fig. 5. Stress-strain curves (a) for the honeycomb compression experiment shown in Fig. 4, (b) for extension of the elastomer at a strain rate of 3.7×10^{-3} s^{-1}.

honeycomb is higher than that of the TPE (Table 1); the approximate Young's modulus of similar polypropylenes is 1.0 GPa. The collapse stress, estimated by eqn (4), is three times the experimental value in both cases, but there is a factor-of-two uncertainty in the result due to face thickness variation.

3. Analysis of in-plane compression

3.1. Analysis of compression in the x-direction

When a honeycomb is uniaxially compressed in the x-direction (Fig. 2a), there is no vertex rotation, due to the symmetry of the structure and the loading. The zero stress in the y-direction means that the faces parallel to y are stress free. There is zero bending moment at the mid-point O of the slanting face BD. Thus only the shape of the half face OB will be analysed, using the method of Zhu et al. (1997) for open cell foams. The moment distribution in OB is the same as if it were a cantilever beam, loaded at the free end by the force P acting in the x-direction (Fig. 2c). The governing differential equation for its shape is

$$EI\frac{\mathrm{d}^2\theta}{\mathrm{d}s^2} = -P\sin\theta \tag{7}$$

where E is the material Young's modulus, and I the second moment of area of the face, s is the curvilinear co-ordinate with origin at O, and θ the angle measured clockwise, between the force axis and the s-axis, at a general point on the face. The boundary conditions are

$$\theta(L/2) = \frac{\pi}{6} \text{ and } M(0) = 0 \tag{8}$$

The elliptical integral $F(\alpha)$ is a function of the value of θ at O

$$F(\alpha) \equiv \int_{\delta}^{\pi/2} \frac{\mathrm{d}\phi}{\sqrt{1 - \sin^2(\alpha/2)\sin^2\phi}} \tag{9}$$

where the lower limit of integration is

$$\delta = \sin^{-1}\left(\sin\frac{\beta}{2}\Big/\sin\frac{\alpha}{2}\right) \tag{10}$$

and ϕ is defined via

$$\sin\theta/2 = \sin(\alpha/2)\sin\phi \tag{11}$$

The face orientation β is $\pi/6$ for regular honeycombs. The force P is related to the elliptic integral by

$$P = \frac{4EIF^2(\alpha)}{L^2} \tag{12}$$

The honeycomb can be divided into units like that outlined by the dashed lines in Fig. 2a. Hence the compressive engineering stress σ_x is given by

$$\sigma_x = \frac{2P}{3bL} \tag{13}$$

where b is the face breadth. For the deformation modes shown in Figs. 2 and 3, the tensile strain ε_x depends on the projected length x_L of CB on the x-axis

$$\varepsilon_x = \frac{x_L^{\mathrm{CB}} - L\cos\beta}{L\cos\beta} \tag{14}$$

The β term is included, so the result applies when the hexagon cell angles are not 120°. The tensile strain in the y-direction depends on the projected lengths of both CB and BA along the y-axis

$$\varepsilon_y = \frac{y_L^{\mathrm{CB}} + y_L^{\mathrm{BA}} - L - L\sin\beta}{L + L\sin\beta} \tag{15}$$

For the mode 1 deformation patterns, the face BA does not deform, so eqn (15) becomes

$$\varepsilon_y = \frac{y_L^{\mathrm{CB}} - L\sin\beta}{L + L\sin\beta}$$

The projected length of the face CB along the x-axis is given by

$$x_L = \frac{L}{F(\alpha)}\sin(\alpha/2)\cos\delta \tag{16}$$

whereas the projected length y_L is given by an elliptic integral (Zhu et al., 1997) as

$$z(\theta) = \frac{L}{2F(\alpha)}\int_{\delta}^{\pi/2}\frac{1-2p^2\sin^2\phi}{\sqrt{1-p^2\sin^2\phi}}\,\mathrm{d}\phi \tag{17}$$

where $p = \sin(\alpha/2)$. To make the results applicable for any relative density R of honeycomb, the reduced

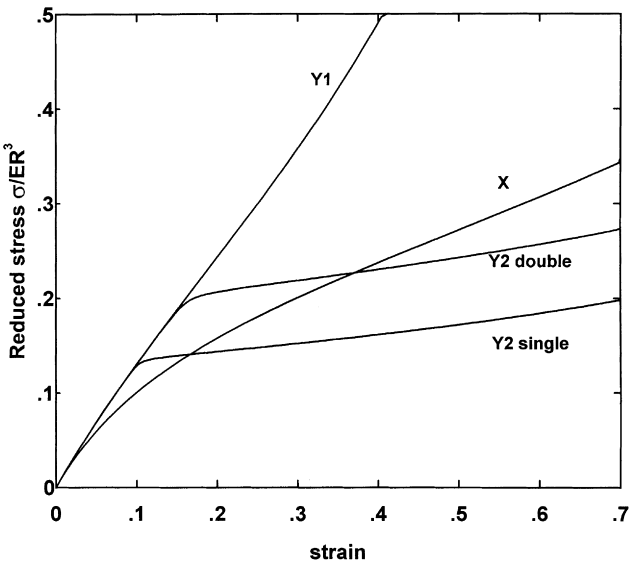

Fig. 6. The predicted reduced stress vs strain relationship for elastic honeycombs, loaded in the x- and y-directions. Mode 2 deformation is preferred for strains exceeding 10% in the y-direction if the vertical faces are single thickness (or 15% for double thickness faces).

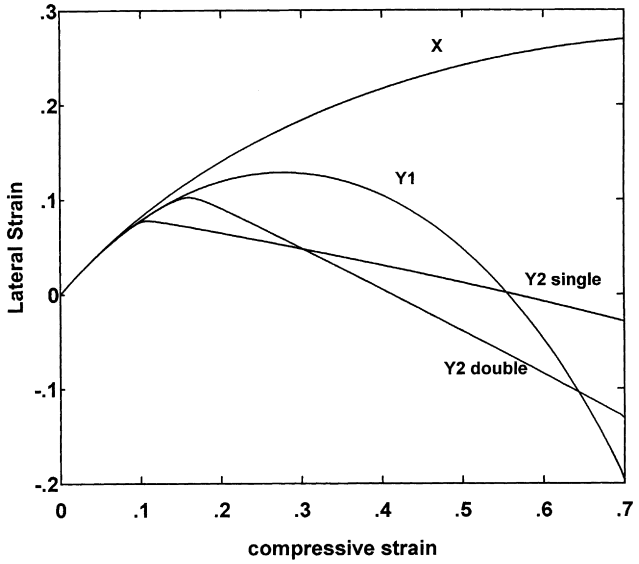

Fig. 7. The predicted lateral strain vs compressive strain relationship for elastic honeycombs, loaded in the x- and y-directions.

stress is defined as the honeycomb stress divided ER^3, i.e. by 2/3 of the honeycomb Young's modulus from eqn (3). Fig. 6 shows that the reduced stress vs strain relationship is non-linear for strains exceeding 5%. The initial slope of the graph is 1.5, as required.

Fig. 7 shows the variation of the lateral tensile strain with the compressive strain, for the three cases of loading. The initial slope of this graph is Poisson's ratio, which has a value of 1 for small strains. The lateral strain is relatively high. It increases monotonically with the honeycomb strain, as slanting faces like CB align towards the y-axis (Fig. 2a).

3.2. Analysis of compression in the y-direction

When honeycomb is uniaxially compressed in the y-direction, two deformation patterns are possible. At a given strain, the deformation pattern that gives the lowest stress will be the one that occurs.

3.2.1. Mode 1 deformation pattern

In this deformation pattern (Fig. 2b), there is no vertex rotation and the vertical faces remain vertical. The elliptic integral solution of the last section can be used with minor modifications. The force on the half face BO is $P/2$ and its initial orientation relative to the y stress axis is $\pi/2-\beta$, or $\pi/3$ for the regular honeycomb. The compressive engineering stress is given by

$$\sigma_y = \frac{P}{\sqrt{3}bL} \tag{18}$$

where b is the face breadth. The strains are still given by eqns (15) and (16), so long as β is taken as the angle between the slanting face and the x-axis.

Fig. 6 shows that the reduced stress vs compressive strain graph is almost linear, despite the fact that faces like BC undergo buckling, becoming S-shaped. The slope of the graph decreases slightly, then

increases for strains exceeding 25%. Part of the faces BC and AE touch when the honeycomb strain is 60%, which means that a more complex calculation would be required for higher strains.

3.2.2. Mode 2 deformation pattern

In mode 2 deformation (Fig. 3) the vertices have the rotation angles $\pm\phi$, with neighbouring vertices rotating in opposite directions. In the computation, the vertex rotations are imposed, and the stresses and strains calculated. The two-dimensional space group of the deformation pattern is pgg, a primitive rectangular lattice with glide planes along both lattice axes (Kelly and Groves, 1970). The consequences are as follows:

1. There are two-fold rotational symmetry axes at the midpoints of the initially vertical faces. Hence the midpoint O of AB is a point of inflection where the moment $M = 0$.
2. The shape of CB is repeated, by a glide axis g_x (translation of half a unit, followed by a reflection) in the x-direction at a level halfway between B and C, to become the shape of BD, etc.
3. The moment on the initially slanting faces varies from M_3 at C to M_2 at B. Since the shapes of CB and BD are the same, the moment variation along them is the same. Hence the forces parallel to the y-axis, acting at B on the ends of BC and BD, must both be $P/2$.
4. Since the x-direction stress is zero, any x-direction compressive force on the face AB must be balanced by an equal x-direction tensile force in the face BD. However the glide plane symmetry in the x-direction means that these forces must be zero.

Therefore only the shapes of the half face BO and the face BC need to be analysed. The forces and moments exerted on them by the vertex B, are shown in Fig. 8. The sign convention, that positive moments cause a beam to hog between supports, is used. The arrows show the directions of positive moments on the faces.

The deformed half face BO has the same bending moment distribution as a cantilever beam, fixed at B and loaded at O by a force P acting in the y-direction. Fig. 8 shows a curvilinear co-ordinate s with origin at O; the clockwise rotation between the stress y-axis and the s-axis is denoted by α. The loading of the half face is identical in type to that in Fig. 2c, and the problem can be solved by elliptic integrals. At a general position s, the bending moment is

$$M_{\mathrm{BO}}(S) = P\int_0^S \sin\alpha \, \mathrm{d}s \tag{19}$$

When evaluated at B, this gives the moment M_1 acting on the end of the face as

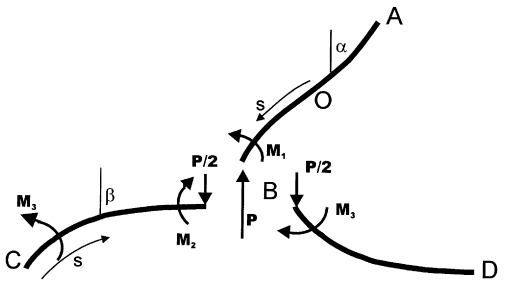

Fig. 8. The forces and moments acting on the faces meeting at the vertex B, for mode 2 compression along the y-axis.

$$M_1 = P\int_0^{L/2} \sin\alpha \, ds \tag{20}$$

If the face remains elastic, the curvature is related to the moment by

$$\frac{d\alpha}{ds} = -\frac{M(s)}{EI} \tag{21}$$

The minus sign arises since the s-axis is oriented towards the left. Since the face orientation at B is ϕ, the orientation elsewhere is given, substituting for the bending moment from eqn (19), by

$$\alpha(s) = \alpha(L/2) + \int_s^{L/2} \frac{M}{EI}\, ds = \phi + \frac{P}{EI}\int_s^{L/2}\left(\int_0^s \sin\alpha \, ds\right) ds \tag{22}$$

The deformed face BC is shown in Fig. 8. A curvilinear co-ordinate s has its origin at C, and the face orientation is denoted by β. A restraining moment M_2 acts at B on the face, so at a general position s, the bending moment is

$$M_{BC}(s) = M_2 + \frac{P}{2}\int_s^L \sin\beta \, ds \tag{23}$$

When evaluated at C the equation gives the relationship

$$M_3 = M_2 + \frac{P}{2}\int_0^L \sin\beta \, ds \tag{24}$$

Fig. 8 shows the direction of the negative moment, of magnitude M_3, which acts on the face BD at B. The three moments acting at B must be in equilibrium, hence $M_1 = M_2 + M_3$. Substituting for M_3 in eqn (24) gives

$$4M_2 + P\int_0^L \sin\beta \, ds = 2M_1 \tag{25}$$

Eqn (22), for the variation of orientation along an elastic face, becomes

$$\frac{d\beta}{ds} = \frac{M(S)}{EI}$$

because the s-axis is oriented towards the right. The face orientation at a general position is therefore

$$\beta(s) = \beta(0) + \frac{1}{EI}\left(M_2 s + \frac{P}{2}\int_0^s\left(\int_s^L \sin\beta \, ds\right) ds\right) \tag{26}$$

Substituting the boundary conditions at C $\beta(0) = \pi/3 - \phi$ and B $\beta(L) = \pi/3 + \phi$ gives

$$2M_2 L + P\int_0^L\left(\int_s^L \sin\beta \, ds\right) ds = 4\phi EI \tag{27}$$

Using eqn (20) to substitute for M_1 in eqn (25) gives an expression for M_2, which when substituted in eqn (27) gives the force

$$P = \frac{8\phi EI}{2L\int_0^{L/2} \sin\alpha \, ds + 2\int_0^L \left(\int_s^L \sin\beta \, ds \right) ds - L\int_0^L \sin\beta \, ds} \tag{28}$$

The face CB and the half face BO are divided into 200 segments, with initial angles $\alpha_0(s) = 0$ and $\beta_0(s) = \pi/3$ for all but the end segments. For given vertex rotations $\pm\phi$, increased in small steps, and the old values of the angles $\alpha(s)$ and $\beta(s)$, the unknowns P, M_1 and M_2 are calculated in turn from eqns (28), (20) and (25) respectively. Using these values, trial values of the angles $\alpha(s)$ and $\beta(s)$ are calculated using eqns (22) and (26). The angles are relaxed slightly towards the trial values, and the process repeated until the solution converges, using the condition that the largest change in any segment orientation in an iteration is 10^{-5} radians. The compressive stress is given by eqn (18) and the strains by eqns (15) and (16).

The predicted variation of the reduced stress vs the honeycomb strain is shown in Fig. 6. The mode 2 reduced stress is imperceptibly larger than that for mode 1 deformation until the strain reaches 9%, and becomes 1% lower at a 10% strain. The rotation angle ϕ is 1° at 9% and 2° at 10% strain, then increases almost linearly with strain, reaching 10° at 13% strain and 26° at 30% strain. When the compressive strain $\varepsilon_y = 0.3$, the predicted shape of the (single thickness) buckled faces is shown in Fig. 3. There is significant curvature visible in the initially vertical faces. This contrasts with the double face thickness case (Fig. 9) where the curvature of these faces is only just detectable. Thus the assumption of Klintworth and Stronge (1988), that these faces do not deform, is reasonable. For double thickness vertical faces, the reduced stress for mode 2 deformation is 1% lower than that for mode 1, when the strain is 15%.

The reduced stress level for elastic collapse increases significantly with strain. This confirms the FEA modelling of Papka and Kyriakides (1994), and shows that the result of Gibson et al. (1982) is a first approximation. The prediction of eqn (4), expressed as a reduced stress for honeycombs with single-thickness vertical faces, is

$$\sigma_{CE} = 0.145ER^3$$

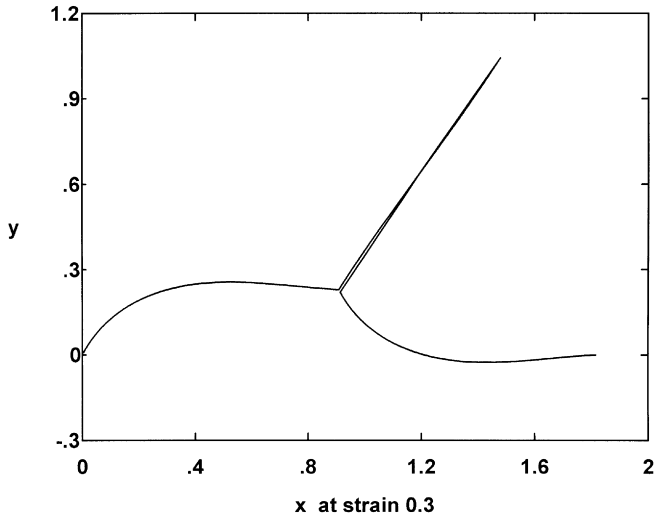

Fig. 9. The predicted shape of a honeycomb with double face thickness vertical faces, at a strain of 30%. There is insignificant curvature in the double thickness faces.

The reduced stress, for the initiation of mode 2 buckling at 10% strain is 13% smaller than this, whereas at 70% strain, when the faces almost touch, it is 37% higher. Klintworth and Stronge's (1988) result for double thickness vertical faces reduces to

$$\sigma_{CE} = 0.213ER^3$$

The initial buckling stress at 15% strain is 12% smaller than this, whereas the value at 70% strain is 30% higher. If the material remains linearly elastic, there is predicted to be a monotonic stress increase throughout the compression range, and this is seen later to preclude the possibility of strain localisation.

3.3. Elastic-plastic response

The moment M_i to initiate yielding in a face of breadth b and thickness t occurs when the strain in the face surface reaches the yield strain, at

$$M_i = \frac{bt^2 Y}{6} \tag{29}$$

where Y is the initial yield stress of the material in tension, and $-Y$ that in compression. If the material is then perfectly plastic with a constant yield stress of $\pm Y$, a plastic hinge forms in the face when the moment is M_H, given by

$$M_H = \frac{bt^2 Y}{4} \tag{30}$$

However, for this moment the curvature becomes infinite, and such a material model can cause instability in the modelling. A more realistic material response was used, with the post-yield part of the stress–strain curve having a constant slope Y_2. Starting with a moment M_i and incrementing it by a factor of 1.05, a table of face curvature vs bending moment was created.

An iterative solution method was used, calculating the moment distribution on the honeycomb faces, then finding the curvature. For the mode 1 y–axis compression, the program is simple. The half face BO is split into 200 segments, at each of which the moment is evaluated by the numerical equivalent of eqn (19), remembering that the force acting is $P/2$. For each increment of stress, the 'old' face shape is used to evaluate the moment distribution. The curvature of each segment is found by interpolating the stored moment vs curvature relationship. If the bending moment is below M_i, eqn (21) can still be used. Trial segment orientations are calculated by integrating the curvature from the vertex B, which does not rotate. The angles are then relaxed from the 'old' to the 'trial' angles, by a factor of about 20%, and the moments re-calculated. The solution converges, and the process stopped when the maximum angle change is less than 0.5 mrad.

For the mode 2 model it is assumed that the initially vertical face BA remains elastic. The problem is to find the force P that causes vertex rotations of $\pm\phi$. Using the value of P from the last strain step, the variation of the bending moment along CB is given by eqn (23), where the value of M_2 is given by eqns (20) and (25). The curvature of the face segments is evaluated, and the total rotation from C to B found by integration, and compared with the target value of 2ϕ. The force value is then stepped in the direction to approach the target. Using the new values of P and M, the shape of the elastic face BO is evaluated using eqn (22). The process is repeated, with the force steps being reduced every time the rotation value overshoots the target. Typically, 30–50 iterations are sufficient to reduce the maximum segment angle change to less than 0.005 radian.

The response of a typical aluminium honeycomb was simulated, using a Young's modulus of 70 GPa,

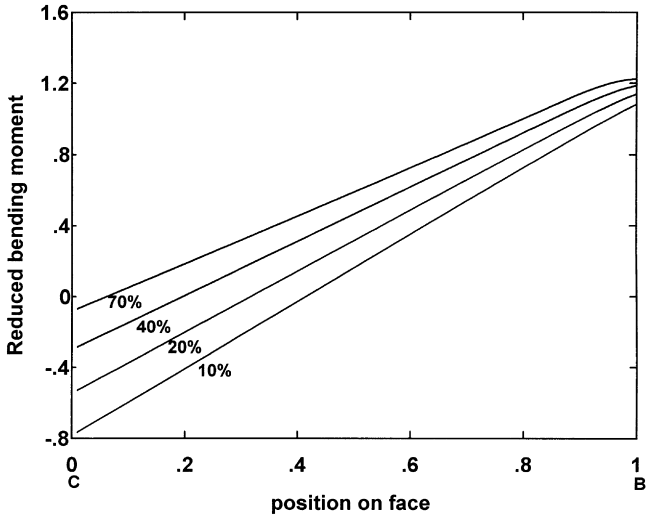

Fig. 10. Bending moment distribution along the face CB as a function of the honeycomb strain, for an aluminium honeycomb with $E = 70$ GPa, a yield strain of 0.5%, and $Y_2 = E/100$.

a yield strain of 0.5% and a post-yield modulus of 0.7 GPa. As the honeycomb strain increases, the bending moment distribution across the face CB changes (Fig. 10). The bending moments are normalised by dividing by the plastic hinge value M_H from eqn (30). In the simulation the rotation of vertex B is negative, so a plastic hinge develops at B, allowing the face CB to rotate relative to the vertex B. The bending moment distribution is initially anti-symmetric along the face, being approximately $-M_H$ at one end and M_H at the other end. As the vertex rotates, the moment M_2 at B increases slightly but the moment M_3 at C falls towards zero. This implies that the moment M_1 on BA

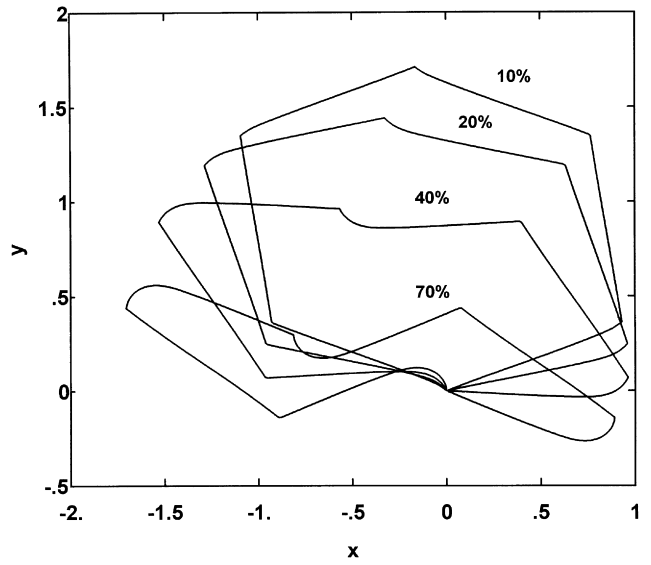

Fig. 11. Predicted cell shapes at compressive strains of 10, 20, 40 and 70%, for the aluminium honeycomb of Fig. 10. The single thickness faces have a thickness to length ratio of 0.03.

Table 2
Predictions of the effects of yielding for mode 2 compression in the y-direction

Material	Vertical faces	Yield strain %	Minimum t/L for plasticity to reduce the collapse stress by 10%
Aluminium	double	0.5	0.0097
Aluminium	double	2	0.038
Polypropylene	single	5	0.14

at B increases. Fig. 11 shows the predicted shape of one cell at a range of compressive strains. As the material yield strain is low the single faces, that were initially vertical, remain underformed. Therefore the result also applies to honeycombs with double thickness faces. There is one plastic hinge near each vertex, and pairs of faces remain connected by a rigid vertex, whereas the mode 1 collapse model of Gibson et al. (1982) there are two plastic hinges at each vertex. The low yield strain means that the single vertical faces remain planar, so the result could apply to a honeycomb with double vertical faces.

For mode 1 compression in the y-direction, material plasticity only affects the collapse stress when the honeycomb density or t/L value is sufficiently high, and/or the yield strain is sufficiently low (Table 2). The polypropylene honeycomb tested has t/L of 0.06, below the limit for a material with a 5% yield strain, so its collapse stress is determined by elastic buckling; whereas that of aluminium honeycombs is determined by plastic collapse.

When the honeycomb cell size is fixed, the face thickness is proportional to the relative density R. As the maximum bending strain e_{bendmax} in the material, at a fixed honeycomb strain, is directly proportional to the face thickness, the ratio $e_{\text{bendmax}}/\text{R}$ is a unique function of the honeycomb strain for elastic materials (Fig. 12). If the material is elastomeric, it does not have a yield strain, but the non-linear stress–strain response means that it is more difficult to predict the elastic collapse stress. The compression of honeycombs becomes more difficult once the faces touch, since the moments on the faces are reduced. This occurs at a strain of about 80% for mode 2 and 60% for mode 1 compression in the y-direction.

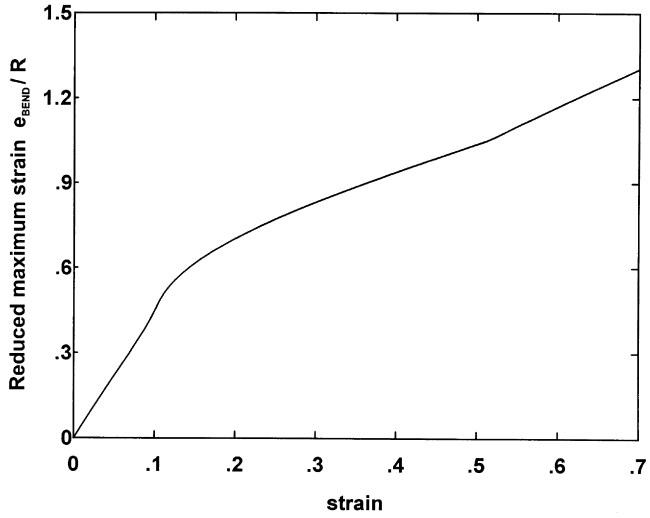

Fig. 12. Reduced maximum face bending strain as a function of the honeycomb strain, for elastic mode 2 deformation in the y-direction.

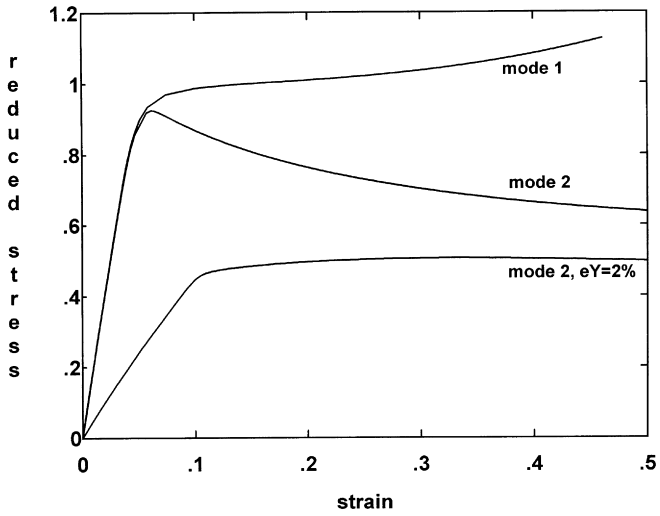

Fig. 13. Reduced stress (stress/collapse stress of eqn (5)) vs strain for honeycombs of $t/L = 0.03$, having single thickness faces, a yield strain of 0.5%, and $Y_2 = E/100$ for both modes of y-axis compression. A mode 2 prediction is also made for a material yield strain of 2%.

The effect of material yielding is to cause the slope of the honeycomb stress–strain graph to fall in the post-yield region. The extent of the change depends on the relative value of the post-yield modulus Y_2. To make the predictions as generally useful as possible, the honeycomb stress is divided by the predicted collapse stress of Gibson et al. (1982) for single face thickness honeycombs—eqn (5)—to provide a reduced stress. However, the result is still a function of the honeycomb relative density, since the pre-yield bending strains are proportional to R. Fig. 13 compares the predicted responses for honeycombs with $t/L = 0.03$ made from an aluminium alloy with $Y_2 = E/100$ and a yield strain of 0.5%. For the mode 1 deformation pattern in the y-direction, the stress still increases after plastic hinges form in the faces, but for mode 2 deformation the stress falls, from 93% of the value from eqn (5) at 6% strain, to 64% of the value when the strain is 50%. The mode 2 deformation, which occurs at a lower stress, will be the operating deformation mode. Eqn (5) provides a reasonable approximation for initial yield stress, but at higher strains collapse occurs at a significantly lower stress level. Fig. 13 also shows a prediction for a material with a 2% yield strain (such as a rigid polymer) with $t/L = 0.03$; the reduced stress is lower than for the aluminium honeycomb, as the faces only begin to yield when the honeycomb strain is 8%. From Table 2 the collapse stress of this honeycomb should be determined by the stress for elastic buckling. The overall response is somewhere between the elastic response of Fig. 6 and the elastic-plastic response of an aluminium honeycomb.

4. Discussion

Face buckling in linear–elastic honeycombs is not necessarily linked to a plateau in the stress–strain curve. For deformation in the x-direction, some faces become S-shaped, yet the slope of the curve remains high. The strain at which mode 2 buckling becomes evident, for compression in the y-direction, is 10% and 15% for single and double thickness vertical faces, respectively. These values are much lower than the 23 to 28% values predicted by Warren et al. (1989) who do not allow the possibility of mode 2 concerted deformation of neighbouring vertices, yet allow hinge points at the face midpoints.

The values agree with the biaxial strain analysis of Hutzler and Weaire (1997) (8% strain for single thickness faces), and the uniaxial result of Papka and Kyriakides (1994) (15% for double thickness faces). The stress–strain curve is linear up to the buckling point, so Gibson and Ashby's (1988) assumption, that the buckling strain can be estimated from the buckling stress and the Young's modulus, is validated.

The mode 2 deformation pattern, with vertices rotating by $\pm\phi$, is the dominant mode of deformation for high strain compression in the y-direction, whether or not the material remains elastic. The collapse stress, estimated by Gibson et al. (1982) for mode 1 plastic deformation, is confirmed analytically as being reasonable for the onset of either mode of elastic-plastic collapse. However the slope of the stress–strain curve at high strains is non-zero, depending both on the geometric non-linearity of the structure and the material non-linearity. Material yielding causes the post-buckling stress to fall, for the mode 2 pattern of y-axis compression, by as much as 30%. The same will occur if the material is non-linearly elastic, with a steadily reducing modulus of the type shown in Fig. 5 for the TPE. There are two reasons why the elastic collapse stresses estimated for the TPE and the polypropylene honeycombs from the initial Young's moduli are too low. Firstly, the effective material Young's modulus when the honeycomb strain is 5% can be significantly lower than the initial modulus. Secondly, strain localisation, initiated from irregularities in the finite size honeycomb, may mean that the collapse stress is that for high strains, without an initial peak of the type in Fig. 13. Silva and Gibson (1997) modelled irregularities in honeycombs, using the Voronoi construction, and showed that the collapse stress was lowered.

A negative slope in the compressive stress–strain curve raises the possibility of strain localisation. Lakes et al. (1993) suggest that if a single cell of an open cell foam has a non-monotonic stress strain curve in compression, there will be localised compression bands in larger foam specimens. Two conditions, necessary for the formation of a localised neck when a thin metal sheet is extended (Reid, 1983), also apply for the formation of a band of highly compressed cells in a compressed honeycomb:

1. The engineering stress must fall in some range of values of increasing stress, so it is possible to have both a high and a low strain at the same value of the applied force. This only occurs for the y-direction mode 2 deformation, when there is material plasticity or non-linearity.
2. The strain, parallel to the band boundaries, must be the same in the highly-deformed band as in the surrounding material. For tensile tests on flat metal specimens, the angle of the neck is at approximately 55° to the tensile axis because Poisson's ratio is effectively 0.5. For the compressed honeycomb, Poisson's ratio is effectively zero, and the band is at 90° to the stress. Fig. 7 shows that, for mode 2 y-axis compression, ε_x remains almost constant with increasing ε_y.

For the strain to change significantly between neighbouring layers of cells, the vertex rotations, on one side of a layer of honeycomb cells, must differ from those on the other side, for the same applied engineering stress. Once a plastic hinge forms near each vertex, the hinge rotation angles can change significantly for a minor change in the stress. Therefore either material plasticity or non-linear elasticity is necessary for the formation of the band of highly compressed cells. The strain localisation pattern observed in the TPE honeycomb is similar to that described for aluminium honeycombs by Papka and Kryiakides (1994). The TPE shows no permanent plasticity, but its response is non-linearly viscoelastic. Hence plasticity as such is not a requirement for strain localisation in honeycombs.

The simplicity of the deformation mechanisms of honeycombs when compressed in-plane means that the effects of material non-linearity can be evaluated, and conditions set for strain localisation. In spite of regular honeycombs being elastically isotropic at small strains, their geometric non-linearity is a function of the compression direction. The response of honeycombs differs from that of open-cell polymer foams. In the latter, the cell edges can twist and bend, making the geometric non-linearity more complex. The simpler topology of honeycombs leads to simpler load paths and an easier explanation of strain localisation.

References

Abd El-Sayed, F.K., Jones, R., Burgess, I.W., 1979. A theoretical approach to the deformation of honeycomb based composite materials. Composites 10, 209–214.

Bitzer, T., 1997. Honeycomb Technology. Chapman and Hall, London.

Gibson, L.J., Ashby, M.F., 1988. Cellular Solids: Structure and Properties. Pergamon Press, Oxford.

Gibson, L.J., Ashby, M.F., Schajer, G.S., Robertson, C.I., 1982. The mechanics of two dimensional cellular materials. Proc. Roy. Soc. Lond. A 382, 25–42.

Hutzler, S., Weaire, D., 1997. Buckling properties of 2D regular elastic honeycombs. J. Physics-Condensed Matter 9, 323–329.

Kelly, A., Groves, G.W., 1970. Crystallography and Crystal Defects. Longman, London, p. 84.

Klintworth, J.W., Stronge, W.J., 1988. Elasto-plastic yield limits and deformation laws for transversely crushed honeycombs. Int. J. Mech. Sci. 30, 273–293.

Lakes, R., Rosakis, P., Ruina, A., 1993. Microbuckling instability in elastomeric cellular solids. J. Mater. Sci. 28, 4667–4672.

Masters, I.G., Evans, K.E., 1996. Models for the elastic deformation of honeycomb. Composite Structures 35, 403–422.

Mills, N.J., Zhu, H.X., 1999. Analysis of the high strain compression of closed-cell foams. J. Mech. Phys. Solids 47, 669–695.

Papka, S., Kyriakides, S., 1998. In-plane compressive response and crushing of honeycomb. J. Mech. Phys. Solids 42, 1499–1532.

Reid, C.N., 1983. Deformation geometry for materials scientists. Pergamon Press, Oxford.

Silva, M.J., Gibson, L.J., 1997. The effects of non-periodic microstructure on the compressive strength of two-dimensional cellular solids. Int. J. Mech. Sci. 39, 549–563.

Timoshenko, S., Gere, 1961. Theory of Elastic Stability. McGraw–Hill, New York.

Warren, W.E., Kraynik, A.M., 1987. Foam mechanics: the linear elastic response of two-dimensional spatially periodic cellular materials. Mech. Mater. 6, 27–37.

Warren, W.E., Kraynik, A.M., Stone, C.M., 1989. A constitutive model for two-dimensional non-linear elastic foams. J. Mech. Phys. Solids 37, 717–733.

Zhu, H.X., Mills, N.J., Knott, J.F., 1997. Analysis of the high strain compression of open-cell foams. J. Mech. Phys. Solids 45, 1875–1904.